NASA Technical Memorandum 101087

Some Notes on Shock Resolving Flux Functions Part I: Stationary Characteristics

Timothy J. Barth

May 1989

National Aeronautics and Space Administration

NASA Technical Memorandum 101087

Some Notes on Shock Resolving Flux Functions Part I: Stationary Characteristics

Timothy J. Barth, Ames Research Center, Moffett Field, California

May 1989

National Aeronautics and
Space Administration

Ames Research Center
Moffett Field, California 94035

SUMMARY

Numerical flux functions for solving the Euler equations using exact and/or approximate solutions of the Riemann problem of gasdynamics are discussed. Under certain restrictive conditions, schemes using these flux functions produce systems of equations which can exhibit a single degree of freedom. In some instances, the solutions represented by this degree of freedom are unstable to perturbations. This local instability can seriously degrade the temporal convergence of numerical schemes. This point is demonstrated by numerical example.

1. INTRODUCTION

A major portion of these notes should be viewed as a review of some known (but perhaps not well known) technical details of flux functions based on approximate and/or exact solutions of the Riemann problem (see van Leer (1984), Roe (1981), Osher and Solomon (1981)). The remainder of these notes describes some anomalous behavior resulting from these constructions. The most remarkable result appears to be that these anomalies can even be found in flux functions which require the exact solution of the Riemann problem.

2. PRELIMINARIES

We consider schemes for solving the one-dimensional inviscid flow equations

$$\mathbf{u}_t + \mathbf{f}(\mathbf{u})_x = 0 \tag{2.1}$$

where $\mathbf{u}$ represents the vector of conserved variables for mass, momentum, and energy. Numerical schemes in semi-discrete form will be assumed to take the following form for the control volume spanning $x_{j-\frac{1}{2}} \le x \le x_{j+\frac{1}{2}}$

$$\frac{d\mathbf{u}_j}{dt} + \frac{\mathbf{h}_{j+\frac{1}{2}} - \mathbf{h}_{j-\frac{1}{2}}}{\Delta x} = 0 \tag{2.2}$$

In this equation, $\mathbf{u}_j$ is the discrete approximation to $\mathbf{u}(x_j)$ and $\mathbf{h}_{j\pm\frac{1}{2}}$ are the numerical flux functions evaluated at the cell-volume interfaces.

In the present analysis we consider several numerical flux functions for solving equation 2.2:

Godunov/Riemann Flux

$$\mathbf{h}(\mathbf{u}^L, \mathbf{u}^R) = \mathbf{f}(\tilde{\mathbf{u}}), \quad \tilde{\mathbf{u}} = \mathbf{u}_{Riemann}(x/t = 0; \mathbf{u}^L, \mathbf{u}^R) \tag{2.3a}$$

S-C-S (Shock-Contact-Shock) Riemann Flux

$$\mathbf{h}(\mathbf{u}^L, \mathbf{u}^R) = \mathbf{f}(\tilde{\mathbf{u}}), \quad \tilde{\mathbf{u}} = \mathbf{u}_{s\text{-}c\text{-}s}(x/t = 0; \mathbf{u}^L, \mathbf{u}^R) \tag{2.3b}$$

Roe Flux

$$\mathbf{h}(\mathbf{u}^L, \mathbf{u}^R) = \frac{1}{2}(\mathbf{f}^R + \mathbf{f}^L) - \frac{1}{2}\text{sign}(A)_{Roe}(\mathbf{f}^R - \mathbf{f}^L) \tag{2.3c}$$

State Fluxes

$$\mathbf{h}(\mathbf{u}^L, \mathbf{u}^R) = \mathbf{f}(\tilde{\mathbf{v}}), \quad \tilde{\mathbf{v}} = \frac{1}{2}(\mathbf{v}^R + \mathbf{v}^L) - \frac{1}{2}\text{sign}(M^{-1}A_{Roe}M)(\mathbf{v}^R - \mathbf{v}^L) \tag{2.3d}$$

In these equations, A is the usual flux Jacobian matrix, $A = \partial\mathbf{f}/\partial\mathbf{u}$. The S-C-S Riemann flux is constructed from elementary wave-transition operators corresponding to compression shocks, entropy-violating expansion shocks, and contact discontinuities. For the state flux, the matrix M is required to satisfy the mean value construction, $\Delta\mathbf{u} = M(\mathbf{u}^R, \mathbf{u}^L)\,\Delta\mathbf{v}$, and pointwise $\mathbf{v} = M^{-1}\mathbf{u}$. This defines a multitude of possible state vectors. For simplicity, we will consider only three such constructions for this flux wherein $\mathbf{v}$ corresponds to the vector of conserved variables $[\rho, \rho u, \rho e]$, vector of primitive variables $[\rho, u, p]$, and Roe's parameter vector $\sqrt{\rho}\,[1, u, H]$.

In the next section the underlying shock structure for these fluxes is reviewed. This is an important aspect of the analysis because this information allows us to clearly identify the underlying degree of freedom (d.o.f.) in the discrete equations when discontinuities are present. By using this information, local stability and convergence characteristics can be explored.

3. REVIEW OF NUMERICAL STATIONARY SHOCK STRUCTURES

In this discussion, the dependent variables are assumed to be piecewise constant and the numerical flux is obtained by solving an exact or approximate Riemann problem centered at each cell face. Rather than consider arbitrary data, left and right state data, $\mathbf{u}^L$ and $\mathbf{u}^R$, are chosen to satisfy the stationary Rankine-Hugoniot jump relations, $\mathbf{f}^L - \mathbf{f}^R = 0$ subject to an intermediate state, $\mathbf{u}^M$, as shown in figure 1.

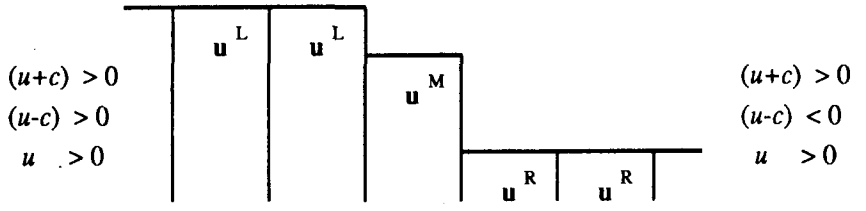

Figure 1. Shock transition profile.

Stationary resolution implies constancy of numerical fluxes.

$$\mathbf{h}^L = \mathbf{h}^{LM} = \mathbf{h}^{MR} = \mathbf{h}^R$$

For numerical fluxes constructed of the form, $\mathbf{h} = \mathbf{f}(\tilde{\mathbf{u}})$, this also implies that

$$\mathbf{f}(\mathbf{u}^L) = \mathbf{f}(\tilde{\mathbf{u}}^{LM}) = \mathbf{f}(\tilde{\mathbf{u}}^{MR}) = \mathbf{f}(\mathbf{u}^R)$$

which requires the simultaneous satisfaction of the stationary jump conditions ($[\mathbf{f}]^{a-b} = \mathbf{f}(\mathbf{u}^b) - \mathbf{f}(\mathbf{u}^a)$)

$$[\mathbf{f}]^{L-LM} = 0, \quad [\mathbf{f}]^{LM-MR} = 0, \quad [\mathbf{f}]^{MR-R} = 0 \tag{3.1}$$

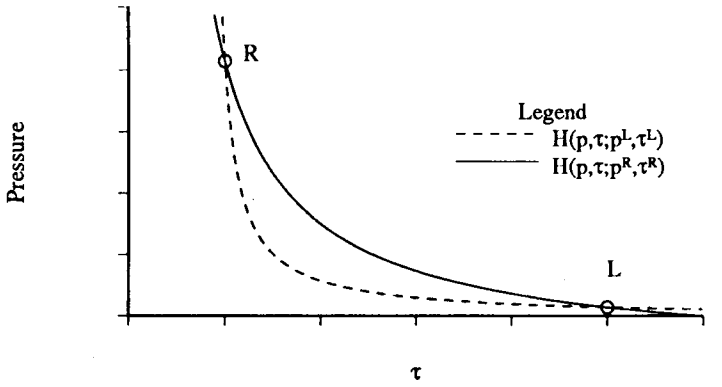

Figure 2. Shock Hugoniot curves.

This occurs only if $\widetilde{\mathbf{u}}^{LM}$ and $\widetilde{\mathbf{u}}^{MR}$ take on either the right or left state values. To see this, consider the implications in the $p-\tau$ plane as shown in figure 2 ($\tau = 1/\rho$). In this figure, the Hugoniot curves, $H(p,\tau;p^L,\tau^L)$ and $H(p,\tau;p^R,\tau^R)$, depict possible shock solutions (moving or stationary) connecting to the left and right states, respectively. The initial data is prescribed such that $H(p,\tau;p^L,\tau^L) \cap H(p,\tau;p^R,\tau^R)$ at the left and right states. Equation 3.1 requires that $\widetilde{\mathbf{u}}^{LM}$ connect to both left and right states by shock solutions. This is satisfied only at the intersection points of the two Hugoniot curves where $\widetilde{\mathbf{u}}^{LM}$ takes on either the left or right state values. To determine which is correct, we look at the functional dependency of the flux state, $\widetilde{\mathbf{u}}^{LM} = \widetilde{\mathbf{u}}(\mathbf{u}^L, \mathbf{u}^M)$. Because we are interested in cases such that $\mathbf{u}^M \neq \mathbf{u}^R$, we conclude that $\widetilde{\mathbf{u}}^{LM} = \mathbf{u}^L$. A similar argument holds for $\widetilde{\mathbf{u}}^{MR}$. For the class of flux functions of the form, $\mathbf{h} = \mathbf{f}(\widetilde{\mathbf{u}})$, the following conditions are necessary for cell equilibrium when $\mathbf{u}^R$ and $\mathbf{u}^L$ connect by a single stationary discontinuity

$$\widetilde{\mathbf{u}}^{LM} = \mathbf{u}^L, \quad \widetilde{\mathbf{u}}^{MR} = \mathbf{u}^R \tag{3.2}$$

This restricts the possible values of $\mathbf{u}^M$. We will use equation 3.2 to show that the numerical scheme, equation 2.2, with Godunov flux function allows resolution of stationary discontinuities with one transition point. The parallel theory for flux functions, equations 2.3b-d, will then be discussed.

Godunov and S-C-S Flux Subcell Wave Structure

The requirement that conditions specified in equations 3.2 are satisfied allows one to obtain qualitative and quantitative information as to the particular waves present in each cell-face Riemann problem as illustrated in figure 3. To gain some insight, we might begin by considering the right cell face and its Riemann problem in the limit as $\mathbf{u}^M$ approaches $\mathbf{u}^R$. In this case, the (2)-(3) waves travel to the right and the (1)-wave travels to the left with speeds approaching their characteristic limits. Before the characteristic limit is reached, the waves would have finite amplitude. Yet the Riemann problem at the right cell face must still produce a state for $x/t = 0$ equal to the right state value, $\mathbf{u}^R$. This can happen only if the amplitudes of the (2)-(3) waves are identically zero.

Now relax the condition that $\mathbf{u}^M$ and $\mathbf{u}^R$ be close together. This wave structure ((2)-(3) waves of zero amplitude) remains valid. If the (1)-wave is a shock, then the jump conditions are satisfied, $[\mathbf{f}]^{M-R} = \sigma\,[\mathbf{u}]^{M-R}$ and valid states, $\mathbf{u}^M$, lie on the Hugoniot curve, $H(p,\tau;p^R,\tau^R)$ connecting $\mathbf{u}^M$ to $\mathbf{u}^R$. Adding the condition that the shock propagate

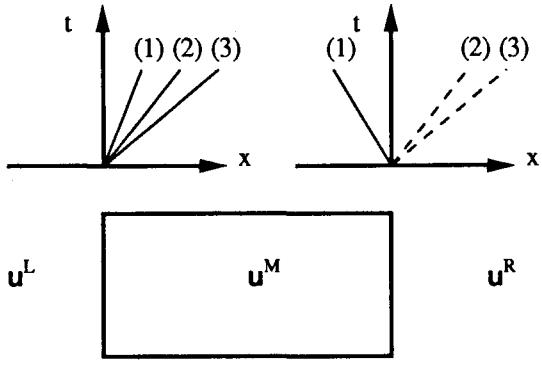

Figure 3. Cell wave schematic for shock transition.

into the cell ($\sigma \leq 0$) we have constraints on ρ, p, and u

$$\rho^L \leq \rho^M \leq \rho^R \tag{3.3a}$$

$$p^L \leq p^M \leq p^R \tag{3.3b}$$

$$u^L \geq u^M \geq u^R \tag{3.3c}$$

The conditions $\rho^M \leq \rho^R$ and $p^M \leq p^R$ ensure that the (1)-wave is a shock and $\rho^L \leq \rho^M$ and $p^L \leq p^M$ ensure that the shock-propagation speed is negative. The bounds on velocity follow from the "mechanical" shock conditions (Courant and Friedrichs, 1948), $G(p,\tau;p^R,\tau^R) = (u-u^R)^2$. If the (1)-wave is a rarefaction, then $(u-c)^M \leq (u-c)^R \leq 0$ (the (1)-wave always travels into the cell) and we obtain limits on ρ, p, and u

$$\rho^L \leq \rho^R \leq \rho^M \tag{3.4a}$$

$$p^L \leq p^R \leq p^M \tag{3.4b}$$

$$u^L \geq u^R \geq u^M \tag{3.4c}$$

As yet, we have not guaranteed that conditions, equation 3.2, on the left cell face are satisfied. Only by considering the left cell-face Riemann problem will we find that not all of these states are possible.

The Riemann problem structure for the left cell face is more complicated. Examining the limit as $\mathbf{u}^M$ approaches $\mathbf{u}^L$, general Riemann problem solutions are possible with all three waves of nonzero amplitude. Conceptually this means that global information concerning the Riemann problem solution is needed. Recall that the solution of the Riemann problem is a composition of elementary wave-transition operators corresponding to shocks, contacts, and rarefactions

$$\mathbf{u}^R = T^{(3)}_{x_3}\ T^{(2)}_{x_2}\ T^{(1)}_{x_1}\ \mathbf{u}^L \tag{3.5}$$

Each transition operator can be constructed as a function of a scalar parameter x. Obtaining a solution of equation 3.5 implies finding the three real valued scalars, x_1, x_2, and x_3. Fortunately, we need determine only x_1 to find all additional constraints on $\mathbf{u}^M$. These

additional constraints will guarantee positive propagation speed of the (1)-wave and, regardless of the particular (2)-(3) waves present, no additional constraints on $\mathbf{u}^M$ can be imposed. The first step is to determine if the (1)-wave is a shock or rarefaction wave. In solving the Riemann problem, equation 3.5, Smoller (1982) reduces the system to solving a single nonlinear equation in x_1. Once x_1 is known, x_2 and x_3 are easily calculated. In his notation we have that the (1)-wave component of the Riemann problem solution is a rarefaction wave if and only if $x_1 \geq 0$ is a solution of

$$\phi(x_1) = h(x_1) + \sqrt{\frac{B}{A}} h(x_1 + \log(B)) = C$$

with

$$h(x_1) = \begin{cases} \frac{2}{\gamma-1}(1 - e^{-\tau x_1}), & x_1 \geq 0 \\ \frac{2\sqrt{\tau}}{\gamma-1} \frac{1-e^{-x_1}}{(1+\beta e^{-x_1})^{1/2}}, & x_1 \leq 0 \end{cases}$$

$$A = \frac{\rho^M}{\rho^L}, \quad B = \frac{p^M}{p^L}, \quad C = \frac{u^M - u^L}{c^L}, \quad \tau = \frac{\gamma - 1}{2\,\gamma}$$

and is a shock otherwise. Independent of which (1)-wave is present on the right cell face, we have, from equations 3.3 and 3.4, $A \geq 1$, $B \geq 1$, and $C \leq 0$. A simple analysis reveals that under these conditions the only solutions of $\phi(x_1) = C$ are for $x_1 \leq 0$ and the left cell-face (1)-wave must be a shock wave. The shock speed in this case is given by

$$\sigma = u^L - c^L \left[\frac{(\beta - 1)z}{\beta - z}\right]^{1/2}$$

with $\beta = \frac{\gamma+1}{\gamma-1}$ and $z = \frac{\beta+e^{x_1}}{1+\beta\, e^{x_1}}$. Positive propagation speed is achieved whenever

$$x_{min} = -\log\left(\frac{(\beta+1)(u^L/c^L)^2 - 1}{\beta}\right) \leq x_1 \leq 0 \tag{3.6}$$

We can readily compute the limit cases of $\phi(x_1) = C$

$$x_1 = \begin{cases} 0, & \mathbf{u}^M = \mathbf{u}^L \\ x_{min}, & \mathbf{u}^M = \mathbf{u}^R \end{cases}$$

The function $\phi(x_1)$ is a monotonically increasing function of its argument and C varies monotonically with u^M. From this we can conclude that $x_{min} \leq x_1 \leq 0$ only for $u^L \leq u^M \leq u^R$. This excludes the right cell-face rarefaction solution. Thus, the only solution remaining connects $\mathbf{u}^M$ to $\mathbf{u}^R$ on the Hugoniot curve, $H(p, \tau; p^R, \tau^R)$, and connects $\mathbf{u}^L$ to $\mathbf{u}^M$ in general by a full three-wave solution of which the (1)-wave must be a shock. This also guarantees bounds on the variables ρ^M, p^M, and u^M

$$\begin{aligned} &\rho^L \leq \rho^M \leq \rho^R \\ &p^L \leq p^M \leq p^R \qquad \text{(Godunov/Riemann flux)} \\ &u^L \geq u^M \geq u^R \end{aligned} \tag{3.7}$$

Without actually knowing the amplitude and/or nature of the (2)-(3) waves on the left cell face, we can consider the picture "complete", i.e., the (2)-(3) waves can add no further constraints on $\mathbf{u}^M$. The remainder of this section will be devoted to a similar analysis of the flux functions (2.3b-d). Since the resultant bounds will be identical to that of the Godunov flux, the reader may wish to proceed directly to section 4 without loss of continuity.

The analysis for the S-C-S Riemann flux follows a similar set of arguments. The right cell-face wave structure connects $\mathbf{u}^M$ to $\mathbf{u}^R$ by a single (1)-wave compression or expansion shock solution. For the (1)-wave compression shock we have the conventional limits

$$\rho^L \leq \rho^M \leq \rho^R \tag{3.7a}$$

$$p^L \leq p^M \leq p^R \tag{3.7b}$$

$$u^L \geq u^M \geq u^R \tag{3.7c}$$

and for a (1)-wave expansion shock we have

$$\rho^L \leq \rho^R \leq \rho^M \tag{3.8a}$$

$$p^L \leq p^R \leq p^M \tag{3.8b}$$

$$u^L \geq u^R \geq u^M \tag{3.8c}$$

As with the Godunov flux, the left cell face also requires knowledge of the global Riemann problem solution. Following a development similar to the conventional Riemann problem, a global solution to this approximate Riemann problem can be constructed. In this case the (1)-wave is an expansion shock if $x_1 \geq 0$ is a solution of

$$\widehat{\phi}(x_1) = \widehat{h}(x_1) + \sqrt{\frac{B}{A}}\widehat{h}(x_1 + \log(B)) = C$$

with

$$\widehat{h}(x_1) = \frac{2\sqrt{\tau}}{\gamma - 1}\frac{1 - e^{-x_1}}{(1 + \beta e^{-x_1})^{1/2}}$$

and is a compression shock otherwise. In this equation we have defined the parameters

$$A = \frac{\rho^M}{\rho^L}, \quad B = \frac{p^M}{p^L}, \quad C = \frac{u^M - u^L}{c^L}, \quad \tau = \frac{\gamma - 1}{2\,\gamma}$$

From equations 3.7 and 3.8, we have, $A \geq 1$, $B \geq 1$, and $C \leq 0$, and all solutions of $\widehat{\phi}(x_1) = C$ are such that $x_1 \leq 0$. As with the Godunov flux, the (1)-wave is a compression shock. Following the same analysis, it follows that positive propagation of the (1)-wave only occurs under the following conditions

$$\rho^M \leq \rho^R$$

$$p^M \leq p^R$$

$$u^M \geq u^R$$

From this constraint the only remaining valid solution connects $\mathbf{u}^M$ to $\mathbf{u}^R$ by a single moving compression shock and connects $\mathbf{u}^M$ to $\mathbf{u}^L$ by a three-wave solution of which the (1)-wave is a compression shock. This wave structure places bounds on ρ^M, p^M, and u^M identical to the Godunov flux

$$\begin{aligned} \rho^L \leq \rho^M \leq \rho^R \\ p^L \leq p^M \leq p^R \qquad \text{(S-C-S Riemann flux)} \\ u^L \geq u^M \geq u^R \end{aligned} \tag{3.9}$$

Roe and State Flux Subcell Wave Structure

The analysis of the Roe and state fluxes is somewhat simpler. These fluxes also have valid intermediate states that connect to the right state by a single moving shock wave. In this discussion we will demonstrate only that this wave configuration does indeed satisfy the conditions for cell equilibrium. From this we will obtain bounds on the $\mathbf{u}^M$ state. Note that from the shock-jump relations and the Roe identities we have ($A_{Roe} = X\Lambda X^{-1}$, $\Lambda = \text{diag}(\lambda_1, \lambda_2, \lambda_3)$)

$$\begin{aligned} \sigma\,[\mathbf{u}] = [\mathbf{f}] &= A_{Roe}\,[\mathbf{u}] \\ \sigma X^{-1}\,[\mathbf{u}] &= \Lambda X^{-1}\,[\mathbf{u}] \\ \sigma\,[\mathbf{w}] &= \Lambda\,[\mathbf{w}], \qquad [\mathbf{w}] = X^{-1}\,[\mathbf{u}] \end{aligned} \tag{3.10}$$

In this form the jump relations are satisfied if and only if for some j

$$\begin{aligned} [w_i] = 0 \quad i = 1,2,3 \quad i \neq j \\ \sigma = \lambda_i \quad i = j \end{aligned} \tag{3.11}$$

From this we have that $\text{sign}(\sigma)\,[\mathbf{w}] = \text{sign}(\Lambda)\,[\mathbf{w}]$ and the following useful relations:

$$\begin{aligned} \text{sign}(\sigma)\,[\mathbf{u}] &= \text{sign}(A)_{Roe}\,[\mathbf{u}] \\ \text{sign}(\sigma)\,[\mathbf{v}] &= \text{sign}(M^{-1}AM)_{Roe}\,[\mathbf{v}] \\ \text{sign}(\sigma)\,[\mathbf{f}] &= \text{sign}(A)_{Roe}\,[\mathbf{f}] \end{aligned} \tag{3.12}$$

When $\mathbf{u}^M$ connects to $\mathbf{u}^R$ by a single moving shock, we have, from equation 3.11, that $(u-c)^{MR}_{Roe} = \sigma$ and from the condition that $\sigma \leq 0$ we can conclude

$$\rho^L \leq \rho^M \tag{3.13a}$$

$$p^L \leq p^M \tag{3.13b}$$

$$u^L \geq u^M \tag{3.13c}$$

The flux formulas (equations 2.3c-d) can now be shown to satisfy the right cell-face requirements (equation 3.2) subject to the constraints (equations 3.13a-c). In this case, $\text{sign}(\sigma^{MR}) = -1$, and from equations 3.12 we have

Roe flux (right cell face):

$$\begin{aligned}\mathbf{h}^{MR} =& \frac{1}{2}(\mathbf{f}^M + \mathbf{f}^R) - \frac{1}{2}\text{sign}(A)_{Roe}(\mathbf{f}^R - \mathbf{f}^M) = \frac{1}{2}(\mathbf{f}^M + \mathbf{f}^R) + \frac{1}{2}(\mathbf{f}^R - \mathbf{f}^M) \\ =& \mathbf{f}^R\end{aligned}$$

State fluxes (right cell face):

$$\begin{aligned}\mathbf{h}^{MR} =& \mathbf{f}(\widetilde{\mathbf{u}}^{MR}) = \mathbf{f}(\mathbf{u}(\widetilde{\mathbf{v}}^{MR})) \\ \widetilde{\mathbf{v}}^{MR} =& \frac{1}{2}(\mathbf{v}^M + \mathbf{v}^R) - \frac{1}{2}\text{sign}(M^{-1}AM)_{Roe}(\mathbf{v}^R - \mathbf{v}^M) = \frac{1}{2}(\mathbf{v}^M + \mathbf{v}^R) + \frac{1}{2}(\mathbf{v}^R - \mathbf{v}^M) \\ =& \mathbf{v}^R\end{aligned}$$

We now consider the left cell face. For Roe's flux we require

$$\mathbf{f}^L = \mathbf{h}^{LM} = \frac{1}{2}(\mathbf{f}^M + \mathbf{f}^L) - \frac{1}{2}\text{sign}(A)_{Roe}(\mathbf{f}^M - \mathbf{f}^L) \tag{3.14}$$

After some rearrangement we obtain

$$[\mathbf{f}]^{L-M} = \text{sign}(A)_{Roe}\ [\mathbf{f}]^{L-M}$$

or in terms of the wave amplitudes

$$[\mathbf{w}]^{L-M} = \text{sign}(\Lambda)\ [\mathbf{w}]^{L-M} \tag{3.15}$$

This equation would be satisfied if $\mathbf{u}^M = \mathbf{u}^R$ and $\mathbf{u}^L$ and $\mathbf{u}^M$ connect by a stationary shock (with $\text{sign}(0) = 1$) or whenever $[\lambda_1, \lambda_2, \lambda_3] > 0$. The former situation is actually a limiting case and both are encompassed by the condition $[\lambda_1, \lambda_2, \lambda_3]^{LM} \geq 0$. This amounts to showing that

$$(u - c)^{LM}_{Roe} \geq 0 \tag{3.16}$$

subject to constraint that $\mathbf{u}^M$ lies on $H(p, \tau; p^R, \tau^R) = 0$ and satisfies the constraints listed in equation 3.13 . The analysis for the state fluxes would be identical and will not be repeated here. Although we do not prove this here, we find that these conditions are satisfied only when

$$\begin{aligned}\rho^M &\leq \rho^R \\ p^M &\leq p^R \\ u^M &\geq u^R\end{aligned}$$

Combining these conditions with equation 3.13 we obtain the now familiar conditions

$$\begin{aligned}\rho^L \leq \rho^M \leq \rho^R \\ p^L \leq p^M \leq p^R \qquad \text{(Roe and state fluxes)} \\ u^L \geq u^M \geq u^R\end{aligned} \tag{3.17}$$

Under these conditions, we have that $\text{sign}(A) = I$ and the requirements for cell equilibrium are satisfied

Roe Flux (left cell face):

$$\begin{aligned}\mathbf{h}^{LM} =& \frac{1}{2}(\mathbf{f}^L + \mathbf{f}^M) - \frac{1}{2}\text{sign}(A)_{Roe}(\mathbf{f}^M - \mathbf{f}^L) = \frac{1}{2}(\mathbf{f}^L + \mathbf{f}^M) - \frac{1}{2}(\mathbf{f}^M - \mathbf{f}^L) \\ =& \mathbf{f}^L\end{aligned}$$

State Fluxes (left cell face):

$$\begin{aligned}\mathbf{h}^{LM} =& \mathbf{f}(\tilde{\mathbf{u}}^{LM}) = \mathbf{f}(\mathbf{u}(\tilde{\mathbf{v}}^{LM})) \\ \tilde{\mathbf{v}}^{LM} =& \frac{1}{2}(\mathbf{v}^L + \mathbf{v}^M) - \frac{1}{2}\text{sign}(M^{-1}AM)_{Roe}(\mathbf{v}^M - \mathbf{v}^L) = \frac{1}{2}(\mathbf{v}^L + \mathbf{v}^M) - \frac{1}{2}(\mathbf{v}^M - \mathbf{v}^L) \\ =& \mathbf{v}^L\end{aligned}$$

4. STATIONARY SHOCK WAVE CHARACTERISTICS

We have shown that all fluxes considered require that the primitive variables be bounded between the left and right states

$$\begin{aligned}\rho^L \le \rho^M \le \rho^R \\ p^L \le p^M \le p^R \\ u^L \ge u^M \ge u^R\end{aligned} \tag{4.0}$$

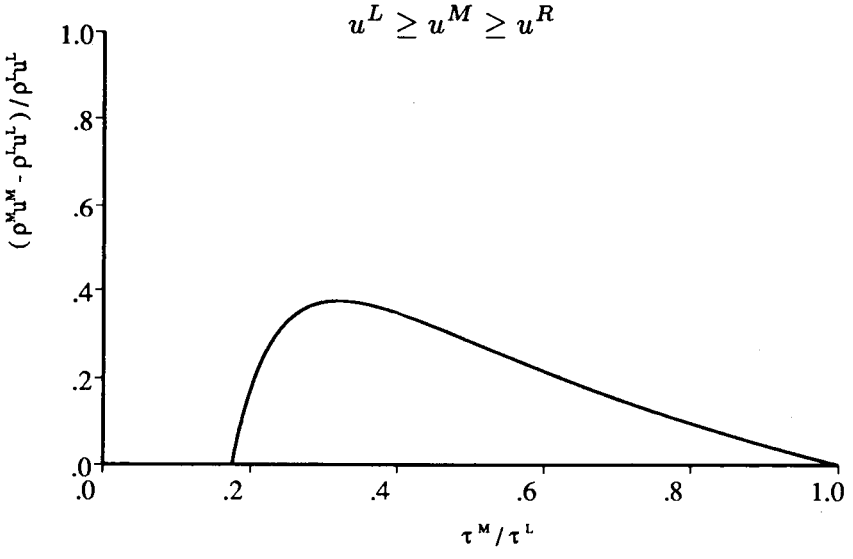

Figure 4. Transition point momentum deviation for M=10 shock.

Note that interval boundedness in primitive variables does not guarantee interval boundedness in other variables. Two obvious examples are momentum and stagnation enthalpy. Across a stationary shock these quantities are constant, yet values at the transition point may deviate significantly

$$\rho^L\, u^L = \rho^R\, u^R \neq \rho^M\, u^M \tag{4.1a}$$

$$H^L = H^R \neq H^M \tag{4.1b}$$

In figure 4 we demonstrate this phenomenon for data corresponding to a Mach 10 stationary shock. In this case we find that, depending on the particular location of the state, $\mathbf{u}^M$, we can have up to a 40% spike in momentum. This can adversely affect some numerical schemes which interpolate/extrapolate state variables and/or other quantities. In part 2 of these notes (T.J. Barth, in preparation), we examine this effect in detail in the context of propagating shock waves.

The wave structure of these fluxes clearly identifies a single d.o.f. present when stationary discontinuities are present. For example, if ρ^M is chosen as the free parameter, then any value can be chosen subject to $\rho^L \leq \rho^M \leq \rho^R$ from which the entire state, $\mathbf{u}^M$, is fixed such that cell equilibrium is satisfied. Pressure is obtained from $H(p,\tau;p^R,\tau^R) = 0$ and velocity from $G(p,\tau;p^R,\tau^R) = (u^R - u)^2$. This d.o.f. implies that the residual function

$$\mathbf{r}(\mathbf{u}^M;\mathbf{u}^L,\mathbf{u}^R) = \mathbf{h}^{MR} - \mathbf{h}^{LM} \tag{4.2}$$

has a singular Jacobian matrix, i.e., $\det(\frac{\partial \mathbf{r}}{\partial \mathbf{u}^M}) = 0$. To see this, construct a vector in state space (ρ,u,p) tangent to the curves, $H(p,\tau;p^R,\tau^R) = 0$ and $G(p,\tau;p^R,\tau^R) = (u^R - u)^2$. Then construct its image, $\mathbf{v}$, in $(\rho,\rho u,\rho e)$ space. From the definition of a Fréchet derivative it can be seen that this vector is an eigenvector associated with a zero eigenvalue

$$\lim_{\epsilon\to 0}\frac{1}{\epsilon}(\mathbf{r}(\mathbf{u}^M + \epsilon\mathbf{v}) - \mathbf{r}(\mathbf{u}^M)) = \frac{\partial \mathbf{r}}{\partial \mathbf{u}^M}\mathbf{v} = 0 \tag{4.4}$$

To understand the consequences of this zero eigenvalue, one might consider solving a system with one interior point, $\mathbf{u}^M$, and boundary data, $\mathbf{u}^L$, $\mathbf{u}^R$

$$\frac{\partial \mathbf{u}^M}{\partial t} + \mathbf{r}(\mathbf{u}^M;\mathbf{u}^L,\mathbf{u}^R) = 0 \tag{4.5}$$

Near a stationary solution, $\mathbf{r}(\mathbf{u}^*;\mathbf{u}^L,\mathbf{u}^R) = 0$, the system can be locally linearized and the solution error, $\mathbf{e} = \mathbf{u}^M - \mathbf{u}^*$, behaves according to the equation

$$\frac{\partial \mathbf{e}}{\partial t} + \frac{\partial \mathbf{r}}{\partial \mathbf{u}^M}(\mathbf{u}^*)\ \mathbf{e} = 0 \tag{4.6}$$

Let $\mathbf{x}_i$ and λ_i denote the *ith* eigenvector and eigenvalue of $\partial\mathbf{r}/\partial\mathbf{u}^M$ at $\mathbf{u}^*$. The solution of equation 4.6 is given by

$$\mathbf{e}(t) = \sum_{i=1}^{3} c_i\mathbf{x}_i e^{-\lambda_i t}$$

where c_i are determined from $\mathbf{e}(0)$. Stability of this equation requires that $\lambda_i \geq 0$. The presence of a zero eigenvalue implies that if the solution is perturbed from a fixed point, $\mathbf{u}^*$, the solution need not return to the same fixed point, but can choose another according to the equation

$$\mathbf{e}(t) = c_1\mathbf{x}_1 + \sum_{i=2}^{3} c_i\mathbf{x}_i e^{-\lambda_i t}$$

For the locally linearized system, we have, from equation 4.4, that $\mathbf{x}_1 = \mathbf{v}$ and the solution is free to move along a local tangent to the shock curves. Note that the singularity of the system does not affect the rate of convergence but merely reflects a d.o.f. Note that this singularity *does* affect algorithms such as Newton's method for solving $\mathbf{r}(\mathbf{u}) = 0$ which require invertibility of the Jacobian matrix. Also note that if we had considered a system consisting of several computational cells in space with a stationary shock somewhere in the interior, the resulting Jacobian matrix would still be exactly singular at the fixed point. The following matrix represents this situation ($T_1 = \partial \mathbf{r}/\partial \mathbf{u}^M$, $|A| = A^+ - A^-$):

$$\begin{bmatrix}
\ddots & & & & & & & & \\
\ddots & A^{+L} & & & & & & & \\
 & -A^{+L} & A^{+L} & & & & & & \\
 & & -A^{+L} & T_1 & T_2 & & & & \\
 & & & -T_1 & T_3 & A^{-R} & & & \\
 & & & & -A^{+R} & |A|^R & A^{-R} & & \\
 & & & & & -A^{+R} & |A|^R & A^{-R} & \\
 & & & & & & -A^{+R} & |A|^R & \ddots \\
 & & & & & & & \ddots & \ddots
\end{bmatrix}$$

This matrix has an obvious partitioning which is block lower triangular and to determine whether this matrix is singular we need only examine the following submatrix:

$$\begin{bmatrix}
T_1 & T_2 & & & & \\
-T_1 & T_3 & A^{-R} & & & \\
 & -A^{+R} & |A|^R & A^{-R} & & \\
 & & -A^{+R} & |A|^R & A^{-R} & \\
 & & & -A^{+R} & |A|^R & \ddots \\
 & & & & \ddots & \ddots
\end{bmatrix}$$

Expanding the determinant of this matrix about the first column, we can easily see that this matrix is singular whenever $T_1 = \partial \mathbf{r}/\partial \mathbf{u}^M$ is singular.

5. SHOCK TRANSITION POINT STABILITY

We have shown which shock structures are possible for the flux functions, equations 2.3a-d; we now check the stability of these solutions to perturbations. Stability requires that the eigenvalues of $\partial \mathbf{r}/\partial \mathbf{u}$ evaluated at the stationary solution are nonnegative. All the fluxes considered have the same one-parameter family of possible solutions, i.e., connect $\mathbf{u}^M$ to $\mathbf{u}^R$ by a single moving shock wave such that the primitive variables are bounded between the left and right states. In the following paragraphs we consider a family of stationary shocks with preshock Mach numbers ranging from 1.5 to 10.0. We then consider varying a parameter, $\tau = 1/\rho$, between its limits. The eigenvalue spectrum of the Jacobian matrix, $\partial \mathbf{r}/\partial \mathbf{u}$, at each state is then calculated. In figures 5,6, and 7 this analysis is carried out for systems

with 1, 3, and 9 cells, respectively, with fixed boundary data, $\mathbf{u}^L$ and $\mathbf{u}^R$. We first verify that one eigenvalue is zero, then we examine the remaining eigenvalues. In particular the minimum eigenvalue (real part) for each case is plotted. As can be seen, the results for the 3 and 9-cell systems are virtually identical, which indicates that all the minimum eigenvalue information is generated in the immediate vicinity of the transition point. Calculations with many more cells have been carried out with identical results. The results for the single-cell calculation differ significantly for all flux functions. This indicates that the interaction with neighboring cells is apparently an important factor in the local stability. The results in figures 5a-f are presented only to show the need for multiple cells in the calculations. The results in figures 7a-f demonstrate the virtual insensitivity to the number of cells (when greater than or equal to 3). We therefore can refer all discussion to figures 6a-f. These plots indicate clearly that for sufficiently strong shocks *all* flux formulæ have regions in which shock transition points are unstable to perturbations. (These occur whenever $\lambda_{min} < 0$.) From these graphs we make the following observation:

For perfect gases ($\gamma = 7/5$), all fluxes considered may have transition states $\mathbf{u}^m$ which are unstable to perturbations when the preshock Mach number is greater than about 6.

It is interesting to note that although the different curves take on different shapes depending on the different flux formula and shock strength, all fluxes cross the zero axis at roughly the same shock strength and values of τ. Since the only common feature of these fluxes is the representation of the wave structure on the right cell face, we conjecture that this may be the ultimate source of these local instabilities. Intuitively this wave structure appears to be the most precarious and the requirement that the (2)-(3) waves have zero amplitude becomes severe as $\mathbf{u}^M$ approaches $\mathbf{u}^L$. When the cell is not in perfect equilibrium, these waves have nonzero amplitude and send wave information to neighboring cells necessary to drive the system toward equilibrium. It appears this process becomes unstable for sufficiently strong shocks.

This phenomenon has important consequences for unsteady calculations involving propagating shocks as well as steady-state calculations. The implications for transient calculations will be presented in part 2 (T.J. Barth, in preparation). The moving shock is related to the stationary shock by a Galilean transformation. In the ideal situation in the limit as the shock speed approaches zero ($\sigma \rightarrow 0$), the transition point approaches a trajectory which moves along the curve $H(p, \tau; p^R, \tau^R) = 0$ from $\mathbf{u}^R$ to $\mathbf{u}^L$ as the shock propagates through a given cell. In the state space and time domain only one trajectory is possible that does not give rise to spuriously generated waves in space. A necessary condition appears to be that all solutions on the curve $H(p, \tau; p^R, \tau^R) = 0$ for (ρ, u, p) between the pre and postshock state must be at least stable in the stationary case. Even this is by no means enough to guarantee that spurious waves are not generated. For steady-state calculations, the results presented in figure 6 indicate that serious problems may arise. Because the local stability characteristics are continuously related to the location of the transition-point, convergence characteristics are strong functions of the transition point location on the shock Hugoniot curve. If the transition-point trajectory is sufficiently close to a region on the Hugoniot curve which exhibits local stability, then the state-space trajectory simply attracts to the

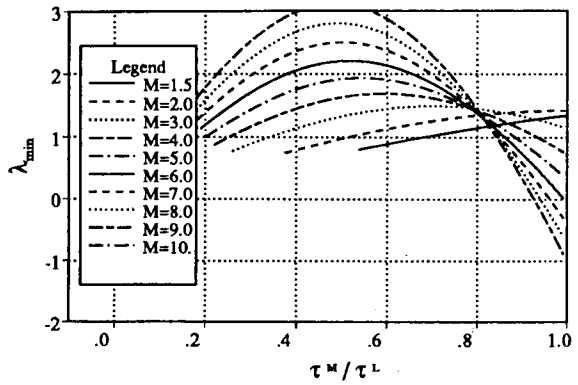

(a) Godunov/Riemann flux.

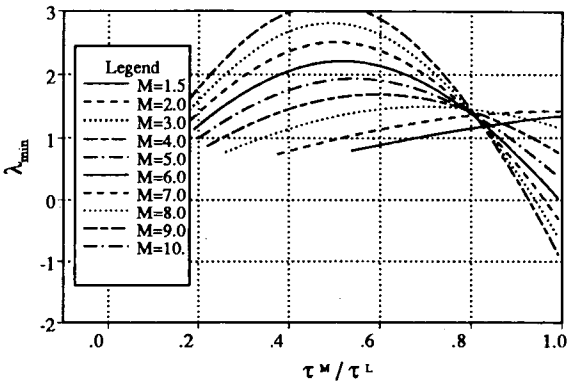

(b) S-C-S Riemann flux.

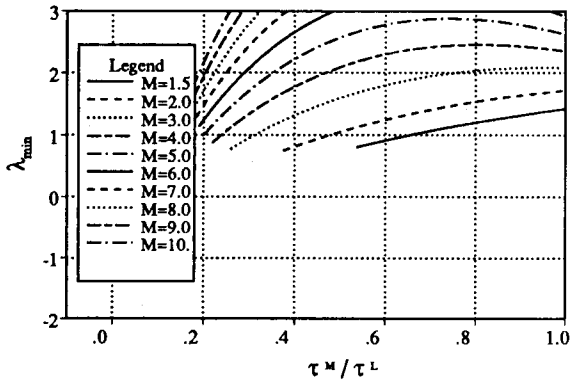

(c) Roe flux.

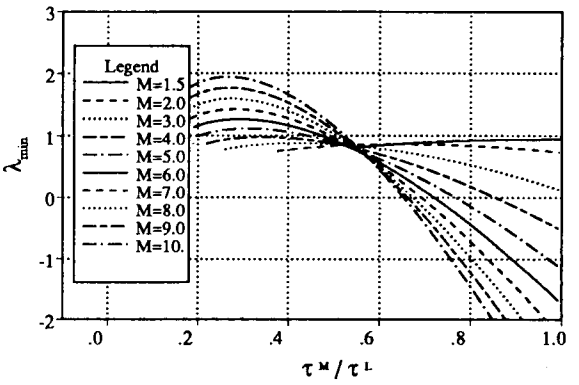

(d) State flux, conserved variables.

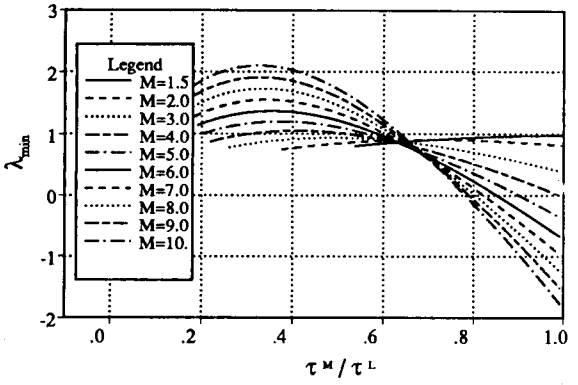

(e) State flux, primitive variables.

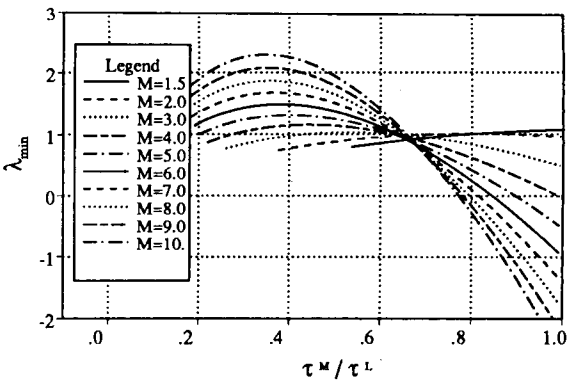

(f) State flux, parameter vector.

Figure 5. Shock wave profile stability – 1 cell ($\gamma = 7/5$).

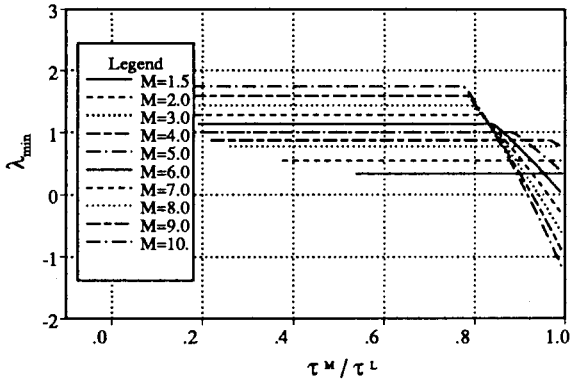

(a) Godunov/Riemann flux.

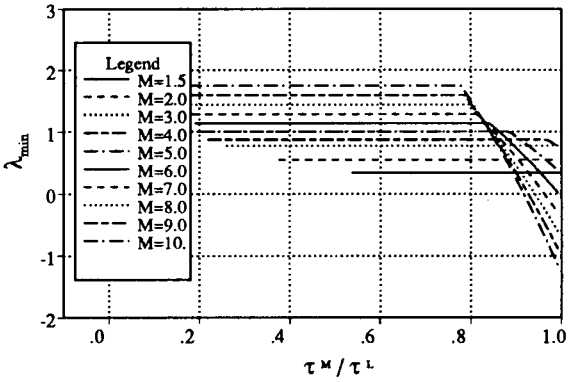

(b) S-C-S Riemann flux.

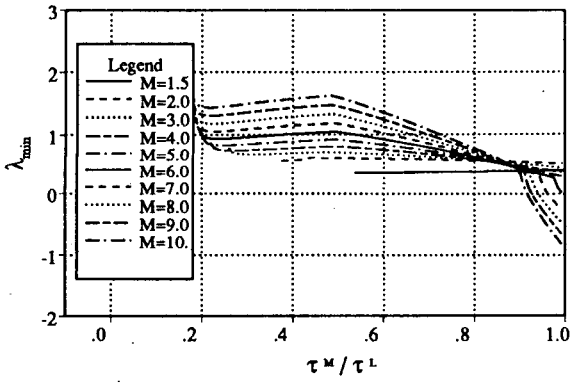

(c) Roe flux.

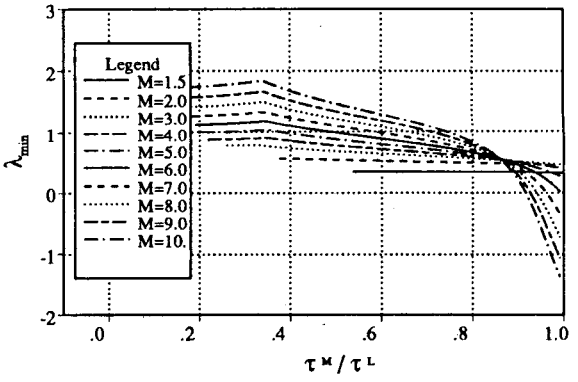

(d) State flux, conserved variables.

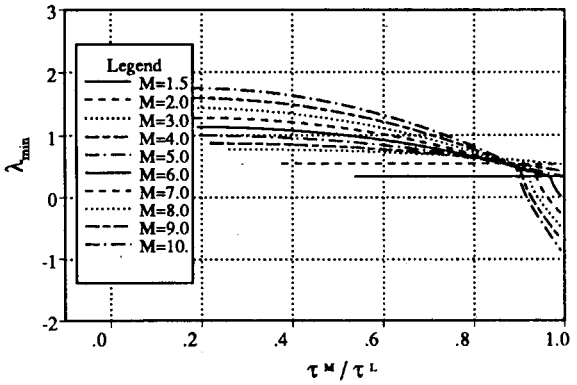

(e) State flux, primitive variables.

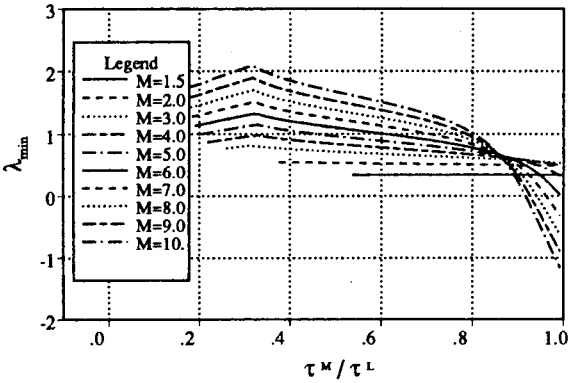

(f) State flux, parameter vector.

Figure 6. Shock wave profile stability – 3 cell ($\gamma = 7/5$).

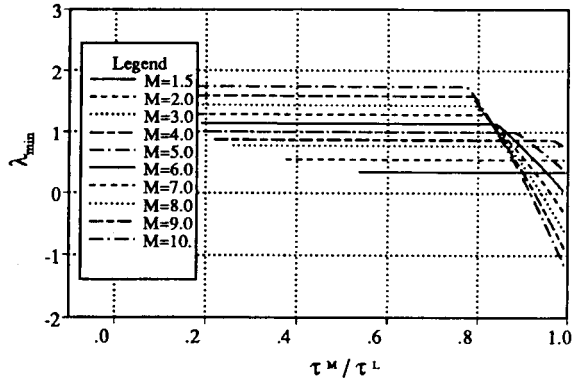

(a) Godunov/Riemann flux.

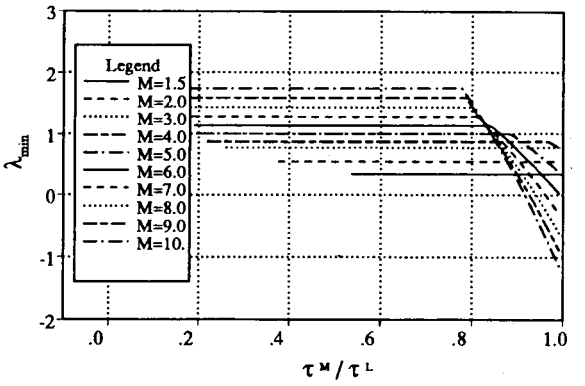

(b) S-C-S Riemann flux.

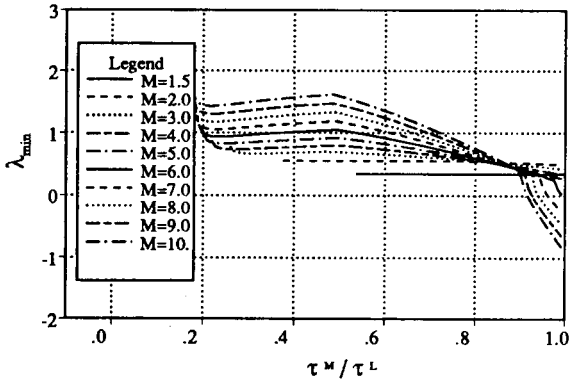

(c) Roe flux.

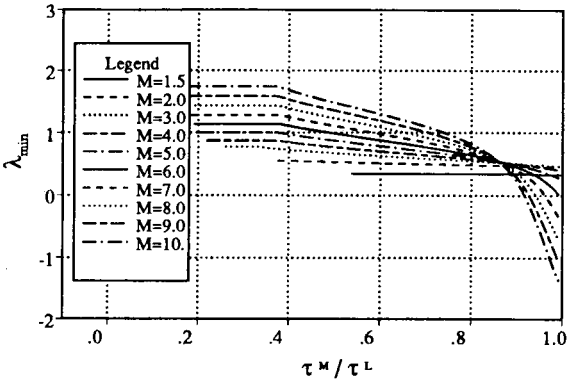

(d) State flux, conserved variables.

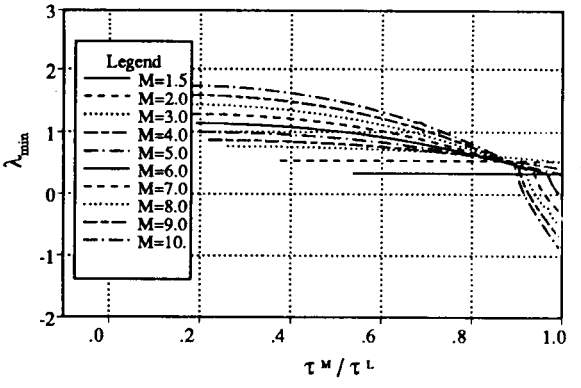

(e) State flux, primitive variables.

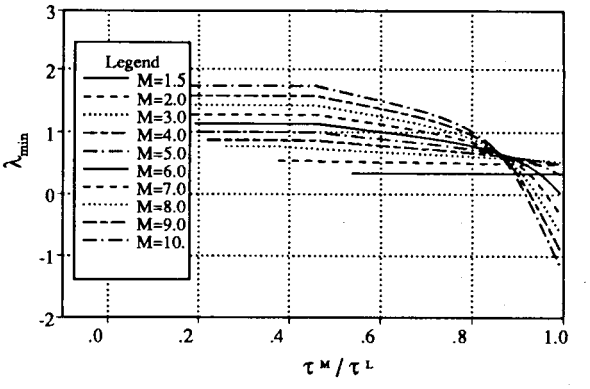

(f) State flux, parameter vector.

Figure 7. Shock wave profile stability – 9 cell ($\gamma = 7/5$).

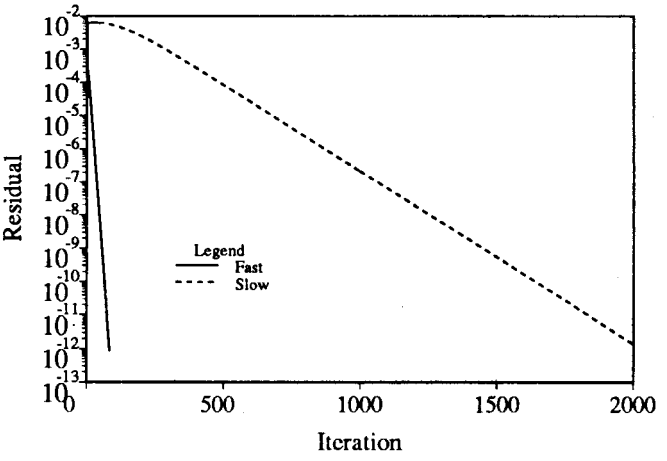

Figure 8. Roe flux convergence histories under two initial conditions.

Hugoniot curve. If the transition-point trajectory is sufficiently close to the region of the Hugoniot curve that exhibits local instability, then the state space trajectory repels from the Hugoniot curve and follows some path, which eventually attracts in a stable region. This process may or may not be much slower than the former process. If the transition-point trajectory is sufficiently close to a region of the Hugoniot curve where $|\lambda_{min}| \leq \epsilon << 1$, then convergence can be extremely slow. For example, if Euler explicit time advancement is used for solving equation 2.2, then the solution converges at a rate proportional to powers of $(1 - \epsilon)$. This is demonstrated in figure 8 for a Mach 8 stationary shock computed using Roe's flux and Euler explicit time advancement on a 19-cell domain. The curves in this figure graph the L_2 norm of the residual as a function of iteration number. After consulting figure 6c, two sets of initial conditions where chosen which nearly satisfy the stationary residual equations. One set of conditions was chosen with the transition point initialized near a region on the Hugoniot curve where $\lambda_{min} \approx 1$. In this case convergence is rapid with the residual dropping 10 decades in about 150 time steps. In the second case the transition point is initialized near a region on the Hugoniot curve where λ_{min} vanishes. Using the same time step as before, over 2000 time steps were required for the same reduction in residual norm. By more careful choice of initial conditions, we have performed calculations requiring over 50000 time steps for the same reduction.

The critical Mach number behavior shows a strong dependence on the ratio of specific heats, γ. In figure 9 this dependence is plotted for several values of γ using the analysis given earlier. Note that for $\gamma \rightarrow 1$, the critical Mach number approaches 3 and for monatomic gases ($\gamma = 5/3$), the critical Mach number is apparently infinite.

6. DISCUSSION

The preceding analysis explains mechanisms which give rise to extremely slow temporal convergence. All fluxes considered indicate that for stationary shocks (with preshock Mach numbers greater than about 6) extremely slow convergence may result. Although we have

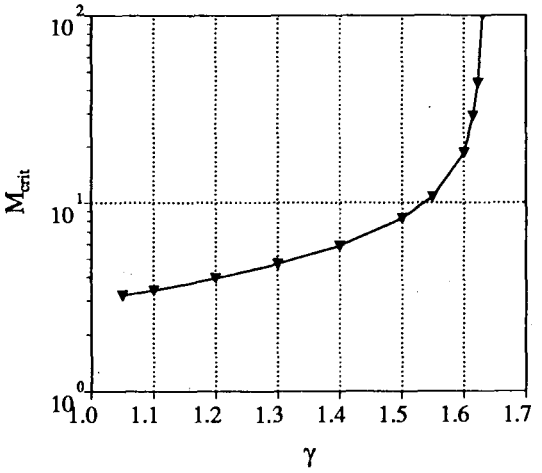

Figure 9. Critical Mach number dependence on gamma.

delayed discussion of slowly propagating shock waves to part 2 of these notes, we note that the stationary properties discussed here can apparently be directly related to anomalies seen in unsteady calculations with propagating shock waves. One consequence discussed in part 2 is the "denting" and "bulging" of slowly propagating shock fronts.

The results presented indicate that renewed interest in flux functions for strong shock waves is needed.

7. REFERENCES

Barth, T. J.: Analysis of Implicit Local Linearization Techinques for Upwind and TVD Algorithms, AIAA-87-0595, Jan. 1987.

Courant, R.; and Friedrichs, K.O.: Supersonic Flow and Shock Waves, Springer-Verlag, 1948.

Roe, P.L.: Approximate Riemann Solvers, Parameter Vectors, and Difference Schemes, J. Comput. Phys., vol. 43, 1981, pp. 357-372.

Osher S.; and Solomon F.: Upwind Difference Schemes for Hyperbolic Systems of Conservation Laws, Math. of Comp., vol. 38, no. 158, 1981, pp. 339-374.

Roe, P. L.: Upwind Differencing Schemes for Hyperbolic Conservation Laws with Source Terms, Lecture Note in Mathematics, vol. 1270, 1987.

Smoller, J.: Shock Waves and Reaction-Diffusion Equations, Springer-Verlag, 1982.

Van Leer, B.: On the Relationship Between the Upwind Differencing Schemes of Godunov, Engquist-Osher, and Roe, SIAM J. Sci. Stat. Comput., vol. 5, no. 1, 1984, pp. 1-20.

NASA
National Aeronautics and Space Administration

Report Documentation Page

1. Report No.	2. Government Accession No.	3. Recipient's Catalog No.
NASA TM-101087		

4. Title and Subtitle

Some Notes on Shock Resolving Flux Functions
Part I: Stationary Characteristics

5. Report Date

May 1989

6. Performing Organization Code

7. Author(s)

Timothy J. Barth

8. Performing Organization Report No.

A-89087

10. Work Unit No.

505-60

9. Performing Organization Name and Address

Ames Research Center
Moffett Field, CA 94035

11. Contract or Grant No.

13. Type of Report and Period Covered

Technical Memorandum

12. Sponsoring Agency Name and Address

National Aeronautics and Space Administration
Washington, DC 20546-0001

14. Sponsoring Agency Code

15. Supplementary Notes

Point of Contact: Timothy J. Barth, Ames Research Center, MS 202A-1
Moffett Field, CA 94035 (415) 694-6740 or FTS 464-6740

16. Abstract

Numerical flux functions for solving the Euler equations using exact and/or approximate solutions of the Riemann problem of gasdynamics are discussed. Under certain restrictive conditions, schemes using these flux functions produce systems of equations which can exhibit a single degree of freedom. In some instances, the solutions represented by this degree of freedom are unstable to perturbations. This local instability can seriously degrade the temporal convergence of numerical schemes. This point is demonstrated by numerical example.

17. Key Words (Suggested by Author(s))	18. Distribution Statement
Euler equations Numerical analysis Riemann problem Roe flux	Unclassified-Unlimited Subject Category – 64

19. Security Classif. (of this report)	20. Security Classif. (of this page)	21. No. of pages	22. Price
Unclassified	Unclassified	21	A02